



Fully Automatic Adaptive Meshing Based Segmentation of the Ventricular System for Augmented Reality Visualization and Navigation

Jesse A.M. van Doormaal¹, Tim Fick², Meedie Ali³, Mare Köllen¹, Vince van der Kuip¹, Tristan P.C. van Doormaal^{1,4}

OBJECTIVE: Effective image segmentation of cerebral structures is fundamental to 3-dimensional techniques such as augmented reality. To be clinically viable, segmentation algorithms should be fully automatic and easily integrated in existing digital infrastructure. We created a fully automatic adaptive-meshing-based segmentation system for T1-weighted magnetic resonance images (MRI) to automatically segment the complete ventricular system, running in a cloud-based environment that can be accessed on an augmented reality device. This study aims to assess the accuracy and segmentation time of the system by comparing it to a manually segmented ground truth dataset.

METHODS: A ground truth (GT) dataset of 46 contrast-enhanced and non-contrast-enhanced T1-weighted MRI scans was manually segmented. These scans also were uploaded to our system to create a machine-segmented (MS) dataset. The GT data were compared with the MS data using the Sørensen–Dice similarity coefficient and 95% Hausdorff distance to determine segmentation accuracy. Furthermore, segmentation times for all GT and MS segmentations were measured.

RESULTS: Automatic segmentation was successful for 45 (98%) of 46 cases. Mean Sørensen–Dice similarity coefficient score was 0.83 (standard deviation [SD] = 0.08)

and mean 95% Hausdorff distance was 19.06 mm (SD = 11.20). Segmentation time was significantly longer for the GT group (mean = 14405 seconds, SD = 7089) when compared with the MS group (mean = 1275 seconds, SD = 714) with a mean difference of 13,130 seconds (95% confidence interval 10,130–16,130).

CONCLUSIONS: The described adaptive meshing-based segmentation algorithm provides accurate and time-efficient automatic segmentation of the ventricular system from T1 MRI scans and direct visualization of the rendered surface models in augmented reality.

INTRODUCTION

Over the last years, 3-dimensional (3-D) techniques such as surgical navigation, augmented reality (AR), and 3-D printing have seen an increase in popularity within medical research. An effective method of image segmentation is fundamental to these techniques. Without a reference to computed tomography (CT), magnetic resonance imaging (MRI), or ultrasound, it is currently impossible to create a realistic 3-D representation of a patient's anatomy. From a user's perspective, image segmentation can be divided in 3 groups. The first is manual segmentation, where an individual draws the contour or

Key words

- Augmented reality
- Image segmentation
- Ventricular system

Abbreviations and Acronyms

2-D: 2-Dimensional

3-D: 3-Dimensional

AR: Augmented reality

AR-HMD: Augmented reality head-mounted display

CNN: Convolutional neural network

CT: Computed tomography

DSC: Dice similarity coefficient

GT: Ground truth

HD₉₅: 95% Hausdorff distance

MRI: Magnetic resonance imaging

MS: Machine segmentation

SD: Standard deviation

STL: Stereolithography

From the ¹Department of Neurosurgery, University Medical Center Utrecht, Utrecht, Province of Utrecht, The Netherlands; ²Department of Neuro-oncology, Princess Máxima Center for Pediatric Oncology, Utrecht, Province of Utrecht, The Netherlands; ³Department of Neurosurgery, Leiden University Medical Center, Leiden, South-Holland, The Netherlands; and ⁴Department of Neurosurgery, University Hospital of Zürich, Zürich, Canton of Zürich, Switzerland

To whom correspondence should be addressed: Jesse A.M. van Doormaal, B.Sc.
[E-mail: Jessevandoomaal@gmail.com]

Citation: *World Neurosurg.* (2021) 156:e9–e24.
<https://doi.org/10.1016/j.wneu.2021.07.099>

Journal homepage: www.journals.elsevier.com/world-neurosurgery

Available online: www.sciencedirect.com

1878-8750/© 2021 The Authors. Published by Elsevier Inc. This is an open access article under the CC BY license (<http://creativecommons.org/licenses/by/4.0/>).

surface of the anatomical region of interest on each scan slice. The second is semiautomatic segmentation, where an individual provides an algorithm with certain clues to support segmentation (e.g., selecting a seed region or drawing an initial contour). The third is automatic segmentation, where an algorithm segments an anatomical region autonomously without any user input.

Accurate segmentation of the ventricular system could provide certain advantages when supporting diagnostics, preoperative planning, or intraoperative navigation. For diagnostics, automated volumetric assessment of each subpart of the ventricles (lateral, third, fourth) would be preferable over subjective 2-dimensional (2-D) measuring over random slices, which is often the current standard. For preoperative planning, difficult anatomical variations (such as in some congenital cases) could be better prepared and understood if a surgeon is provided with a detailed 3-D model of the anatomical region of interest, especially when combined with AR or 3-D printing. Moreover, 3-D models are an asset in the education of patients, residents, or medical students, as 3-D images are more effective to develop spatial understanding than 2-D images.¹⁻⁷ For intraoperative navigation, the model of the ventricle or the trajectory to the chosen entry site of the ventricle could be used to guide a surgeon during ventricular drain placement. Combining this with an augmented reality head-mounted display (AR-HMD) would allow one to superimpose the 3-D model over the real patient.^{8,9}

However, manual segmentation of the ventricular system is time-consuming and impractical work. Therefore, before complex 3-D-based techniques can reach their full potential in neurosurgical practice, automatic machine segmentation (MS) algorithms should be developed. Such algorithms should be fast and accurate to be integrated within a surgeon's daily routine. Within the neurosurgical field, automatic thresholding algorithms are already clinically available to segment certain anatomical structures that are easily distinguishable, such as skin on MRI or the skull on CT. Semiautomatic methods such as locally expanding brushes are often used to segment more complex structures such as the ventricular system or tumors. Several MS algorithms for these more complex structures have been described in literature, often using convolutional neural network (CNN)-based methods¹⁰⁻¹⁶ or atlas-based methods.^{10,17-21} Options for automatic segmentation of the ventricular system provided accurate segmentations^{10,12,14-16,19} but are often still in a proof-of-concept phase and too complex or impractical to use in clinical practice.

We created a cloud-based, AR-accessible automatic segmentation algorithm for the segmentation of the skin, brain, tumors (if applicable), vasculature, and ventricles from T1-weighted MRI sequences. In this study, we focus on the segmentation of the ventricular system. The algorithm's accuracy and segmentation time was tested by comparing it to a manually segmented ground truth (GT) dataset.

METHODS

Ethics

All data were anonymously collected from the University Medical Centre Utrecht (The Netherlands) and University Hospital Zürich (Switzerland). For the data collected from the University Medical Centre Utrecht, images were acquired, anonymized, and stored in

a secured database by the University's clinical trial bureau. For the data collected from the University Hospital Zürich, data were anonymously collected from the institutional ongoing prospective patient registry as approved by the local ethics committee (KEK 2017-01120). All segmentations and MRI sequences were anonymously and securely stored in the cloud environment, which used Azure-based security services (Azure; Microsoft, Redmond, Washington, USA).

Digital Imaging and Communications in Medicine Input

From both study centers, 46 T1-weighted MRI scans from patients admitted for intracranial surgery were included (Table 1). Of these 46 scans, 24 scans (52%) were nonenhanced and 22 scans (48%) were contrast-enhanced (gadolinium). A tumor was present in 19 (41%) of the 46 scans. Scans were classified according to presence of a tumor and width of the third ventricle.

Manual Segmentation

A GT set was constructed from the included MRI scans using an open-source image analysis and segmentation software package (3D slicer, version 4.10.2; Harvard University, Cambridge, Massachusetts, USA). For this dataset, the ventricular system of each MRI scan was manually painted using a "brush" tool on a slice-by-slice basis (Figure 1A). After segmenting all slices of a scan, the volumetric 3-D segmentation was exported in Neuroimaging Informatics Technology Initiative file format. The segmentation was also converted to a 3-D surface model and exported in stereolithography (STL) file format. Segmentations were performed by 1 of 4 authors (J.v.D., M.A., M.K., V.v.d.K.). To optimize the accuracy of each segmentation, a written guideline (Appendix 1) was established that dictated exactly which anatomical structures to include in the segmentation. Furthermore, difficult cases were discussed collectively in a weekly meeting. As final step, all cases were evaluated and corrected slice by slice by the senior author (T.v.D.). If the segmentation was deemed of sufficient quality, the segmentation was included for quantitative analysis.

Automatic Segmentation

The segmentation system was embedded within an online cloud environment that stored all segmentation data (AugSafe; Augmedit, Naarden, The Netherlands). This environment was built, secured and hosted using a cloud computing service (Azure). To use the cloud environment and segmentation algorithm, a web-based user interface was developed which could be accessed using a personal computer or an AR-HMD (Hololens; Microsoft) (Figure 2). Using this interface, MRIs were uploaded in Digital Imaging and Communications in Medicine format and subsequently automatically segmented on an external server that supported simultaneous computation of multiple segmentations.

The automatic segmentation was performed using an expanding mesh algorithm (Disior, Helsinki, Finland). This algorithm uses 3-D adaptive spheres that expand and capture the radiological boundaries of various tissues, including the ventricles. For each scan, this algorithm is tailored to the specific patient by preprocessing using region, threshold and histogram-based segmentation methods. Previously, this method has been used in orbital volume calculations.²²⁻²⁷ Each included scan was sequentially segmented using this system. After segmentation, the mesh

Table 1. Summary of Imaging Characteristics

Imaging Characteristics	
Total number of scans	46
Sequence	
T1 with contrast	22
T1 non-contrast-enhanced	24
Resolution	
192*256	1
201*253	1
225*253	1
240*240	2
256*256	8
288*288	1
320*320	3
236*236	1
336*336	1
400*400	13
464*512	1
471*471	1
480*480	2
512*512	10
Number of slices	
96–150	4
150–250	19
250–350	11
350–400	12

was automatically simplified to streamline 3-D rendering. All segmentation steps were performed without any user input.

The web-based interface was used to access all segmentation results in a 3-D viewer (Figure 1B-C). Within this viewer, individual segmentation components could be made transparent, the segmentation contour could be compared to the scan and the volume of segmentation components could be calculated using a voxel-based method. This interface and the 3-D viewer could also be directly accessed through the AR-HMD (Figure 1D). The cloud contained data converters, simplification algorithms, smoothing algorithms, and 3-D shaders to optimize 3-D models for the AR-HMD. For further analysis, a volumetric 3-D model of each segmentation was exported in binary file format using the web-based application. Additionally, a 3-D surface model of each segmentation was exported in STL file format.

Comparison

For the analysis of segmentation accuracy, the GT group and the MS group were compared using pairwise volumetric and surface statistics. For volumetric analysis, we used the exported

Neuroimaging Informatics Technology Initiative and binary data for the GT and MS group respectively. For surface-based analysis, we used the exported STL data for both groups.

For the volumetric comparison, we used the Sørensen–Dice similarity coefficient (DSC).²⁸ This statistic can be described using the formula:

$$DSC = \frac{2|MS \cap GT|}{|MS| + |GT|}$$

Whereas MS represents the automatically segmented set and GT represents the GT set. This statistic calculates the quotient of similarity between 2 volumetric sets with a value between 0 and 1. A DSC of 1 represents a perfect segmentation, whereas a DSC of 0 represents no overlap at all between the MS and GT data.

For the surface-based comparison, we used the 95% Hausdorff Distance (HD₉₅),²⁹ which can be described using the formulas:

$$h_{95}(MS, GT) = {}^{95}K_{f \in MS}^{th} \min_{g \in GT} \|g - f\|$$

$$HD_{95}(MS, GT) = \max\{h_{95}(MS, GT), h_{95}(GT, MS)\}$$

Whereas MS represents the surface of the machine-segmented set and GT of the GT set. This metric calculates the 95th percentile of the set of distances between points in either the MS or GT set and the closest point of the other dataset (h_{95}). The resulting HD₉₅ value is the highest of both outcomes. HD₉₅ is a measure of the largest segmentation error in mm (after excluding the upper 5% of distances) and is more sensitive for morphologic faults of the segmentation without significant volumetric impact, while minimizing the impact of outliers caused by noisy data. All calculations as described were performed using a custom script written in a computing environment (MATLAB; MathWorks, Natick, Massachusetts, USA).

For the comparison of segmentation time, the time to completion for both the MS and GT data was measured. For the MS data, an automatic timer was implemented that measured the time from the moment the external segmentation server received the MR images up until the moment the server transferred the segmented data back to the cloud environment. As it is not possible to run only individual components of the segmentation algorithm, this timeframe also included segmenting the skin, brain, tumors (if applicable) and vasculature. For the GT data, each researcher measured the time from the moment the MR images were loaded in the segmentation software up until the moment they deemed the segmentation of sufficient quality.

Statistics

For all statistical analyses, extreme outliers were excluded as these were caused by a failure in the segmentation algorithm and are thus not representative of the true performance of the algorithm. To analyze the influence of the presence of tumors on the DSC score, a Mann–Whitney U test was performed to compare the mean DSC scores for the cases that included a tumor and the cases that did not include a tumor. To analyze the influence of third ventricle width on the DSC score, linear regression was performed to compare third ventricle size with DSC scores. P values less than

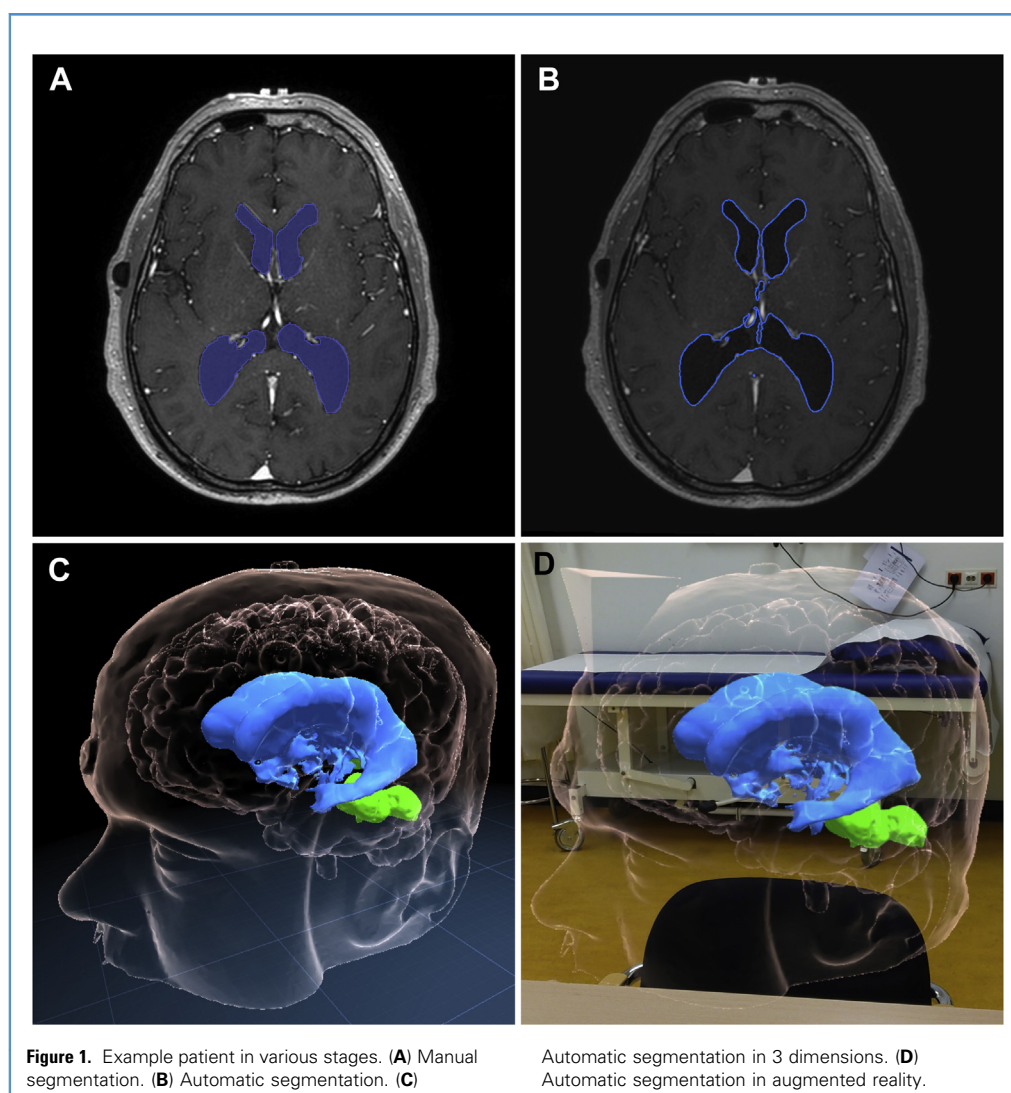


Figure 1. Example patient in various stages. (A) Manual segmentation. (B) Automatic segmentation. (C)

Automatic segmentation in 3 dimensions. (D) Automatic segmentation in augmented reality.

0.05 were considered significant. All aforementioned analyses were performed using a statistical software package (SPSS Inc.; IBM Corp., Armonk, New York, USA).

RESULTS

In total, 46 scans were included, whereof 45 (98%) scans were successfully segmented and computation failed for 1 (2%) case, which failed due to a data reading error. The DSC scores of the 45 remaining scans included 3 extreme outliers, which were excluded from further statistical analysis using DSC. In the sample of 42 remaining scans included for statistical analysis, DSC was negatively skewed with a mean of 0.83 (standard deviation [SD] = 0.08) and median of 0.86 (interquartile range = 0.10). Three examples of segmentations of varying quality are provided in Figure 3.

When we compared the median DSC score of the cases with tumors (median = 0.83) with the median DSC score of the cases

without a tumor (median = 0.88) using a Mann–Whitney U test, there was no significant difference between groups ($U [N_{\text{tumor}} = 17, N_{\text{no tumor}} = 25] = 140, P = 0.06$). Linear regression was performed to estimate the influence of third ventricle width on the DSC. A significant regression equation was found ($F [1,39] = 5.213, P = 0.03$) with an R^2 of 0.343. Predicted DSC is equal to $0.784 + 0.005$ per millimeter third ventricle width. This implies that, on average, a larger third ventricle size causes a greater DSC score.

Of the 45 scans, HD_{95} was positively skewed with a mean of 19.06 mm (SD = 11.20) and median of 16.21 (interquartile range = 13.08). When we considered surface-based metrics, segmentation was least accurate around the third ventricle, due to false-positive inclusion of the ambient cistern and interpeduncular cistern (Figure 4).

Segmentation time was significantly longer for the GT group (mean = 14,405 seconds, SD = 7089) when compared with the MS



Figure 2. Cloud interface as seen through augmented reality head-mounted display. All visible patient information is pseudonymized.

group (mean = 1275 seconds, SD = 714) with a mean difference of 13,130 seconds (95% confidence interval 10,130–16,130).

DISCUSSION

Summary

In this study, we developed and tested a cloud-based adaptive meshing-based segmentation method for contrast-enhanced and non-contrast-enhanced T1-weighted MRI scans, which can be used for 3-D assessment of the ventricular system in AR. We evaluated the accuracy of this system by comparing it to GT segmentations using volumetric and surface-based outcome parameters. The automatic segmentation had a mean DSC score of 0.83 and mean HD₉₅ of 19.06 mm, and was performed in 21 minutes and 15 seconds on average.

Recent Literature

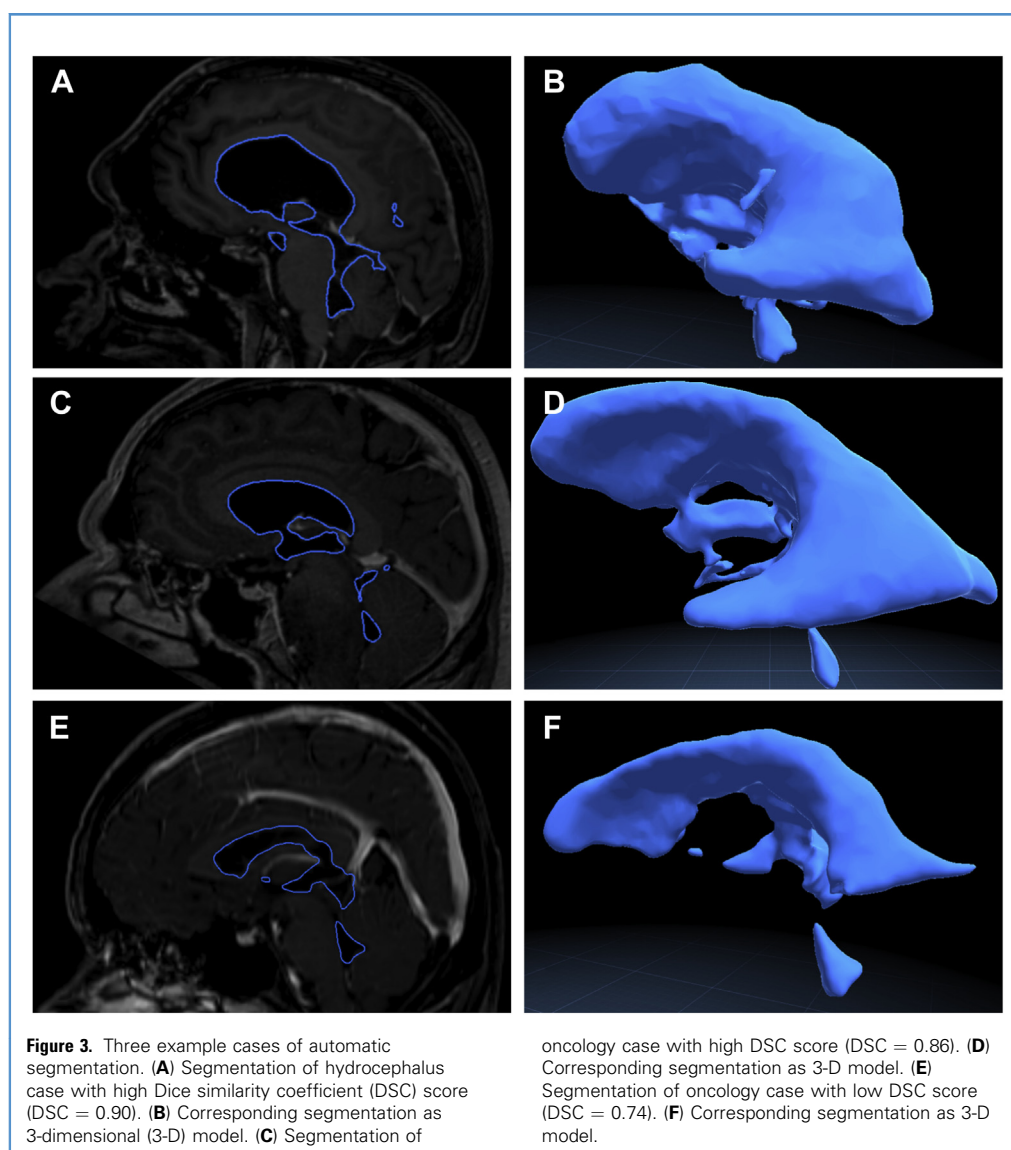
Very frequently, studies that describe automatic segmentation use CNNs.^{10–16} CNNs are generally fast and accurate but also heavily dependent on the quality and size of its training set. A training set needs to be adequately sized before segmentation accuracy is acceptable. In addition, a training set that is not representative of the true patient population may cause lower segmentation accuracy or even failure when applied to patients with pathology such as hydrocephalus.³⁰ Similarly, a training set with no

contrast-enhanced images can cause lower accuracy or failure when using contrast-enhanced images.¹⁰ Reported DSC scores of CNNs for the ventricular system range between 0.89 and 0.97.^{12,14–16}

Alternatively, several studies describe segmentation using atlas-based methods.^{10,17–21} Atlas-based methods are often advantageous when segmenting images with major anatomical variations.³¹ However, atlas-based methods are very dependent on the quality of the atlas set and registration method and can be computationally expensive.^{10,31} Reported DSC scores of atlas-based methods for the ventricular system range between 0.83 and 0.95.^{10,19}

Limitations

In conclusion, compared with CNN or atlas-based methods, the DSC score of our system is at the lower end of the distribution of DSC scores reported in literature. We believe this is caused by a multitude of factors. Notably, most studies only segmented the lateral ventricles, as opposed to including the third and the fourth. Due to the larger volume of the region, the lateral ventricles are easier to segment than the third and the fourth ventricle. Furthermore, not all studies included a dataset with varying degrees of ventricle size and compression. However, the lower segmentation accuracy is also caused by some flaws in our algorithm. We noticed that in the region of the ambient cistern,



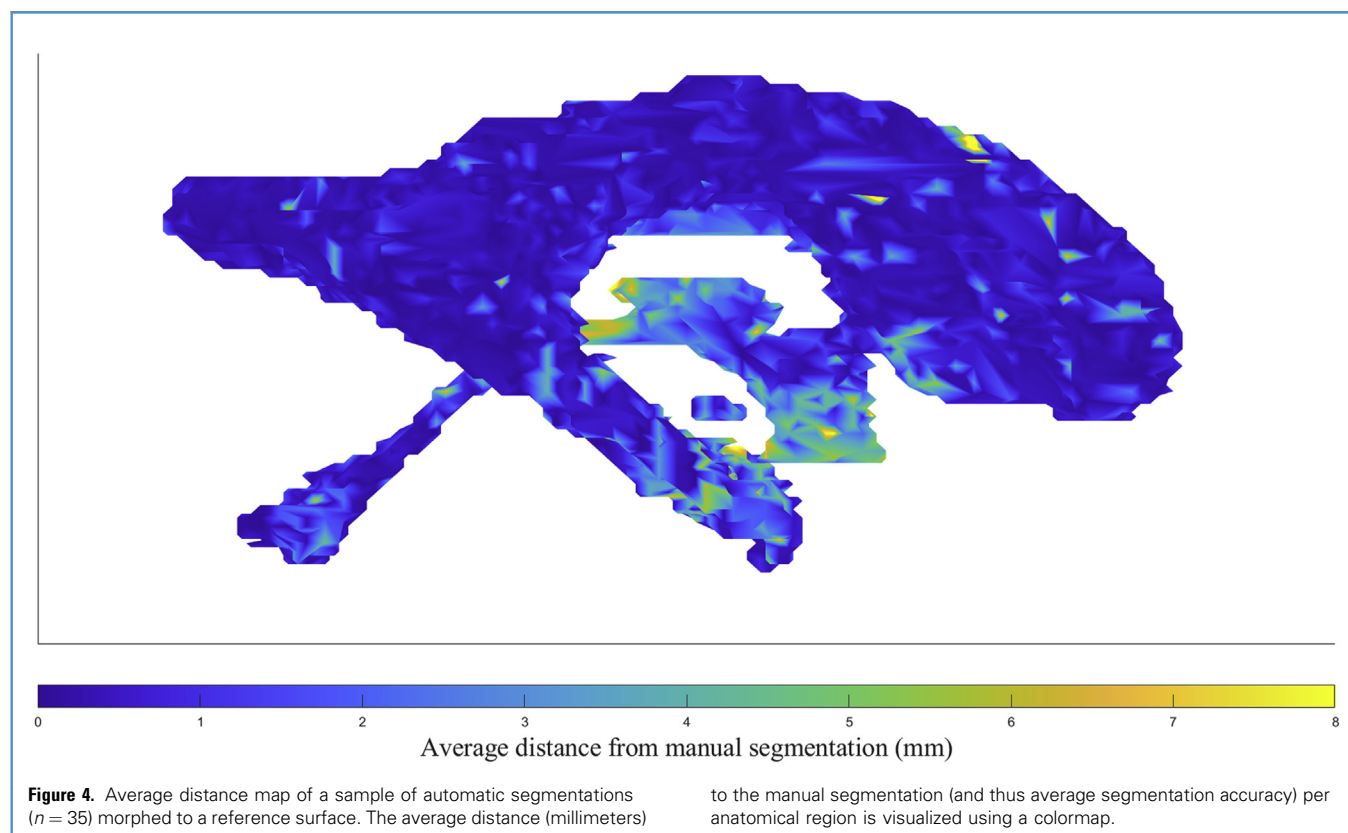
interpeduncular cistern and chiasmatic cistern, the segmentation is susceptible to “leaks.” This causes the algorithm to include these regions in the segmentation as false positives.

An additional element of the algorithm that we strive to improve in the future is its poor adaptation to pathology within the intraventricular volume (e.g., intraventricular hemorrhage or intraventricular tumors). The main cause of this limitation is that parameters such as sharpness of contour, size, position, and intensity value of these structures vary strongly between different patients and within the same patient at certain points in time, especially in case of hemorrhage. This problem is larger in scans without contrast. For technically identical reasons, the algorithm inaccurately includes the choroid plexus in the ventricle segmentation in images without contrast.

A disadvantage of our study methodology is the performance of only one manual segmentation per scan to establish the GT dataset. Generally, the accuracy of a GT dataset can be further enhanced by performing multiple segmentations per case. Nonetheless, we optimized the GT dataset accuracy by establishing segmentation guidelines before the experiment, discussing difficult cases collectively and having each slice evaluated and corrected by the senior author. Taking into account the relative simplicity of segmenting the ventricles, we believe this has established a GT dataset of high quality.

Advantages

Although the DSC is not superior, our system has a number of benefits compared with reported algorithms in the literature. First,



accuracy of segmentation was not influenced by presence of tumors and larger-sized ventricles lead to a greater segmentation accuracy, which allows usage for a broad scope of clinical cases. Second, the system is very well suited for noisy data and anatomical regions with poor contrast. This also facilitates low-resolution scans or difficult anatomical regions such as the third ventricle. Third, the segmentation is relatively fast. On average, a complete segmentation of a scan (including skin, brain, tumor, and vasculature) cost 21 minutes and 15 seconds, which was approximately 11 times faster than manual segmentation. Although recent literature on segmentation using atlas-based methods and CNNs do not report segmentation time, open-source atlas-based packages such as FreeSurfer report segmentation times of multiple hours per case.³²

Finally, our system is fully automatic and runs cloud-based. This allows complete back-end segmentation without requiring input of a user. This eliminates the requirement that specialized personnel spend valuable time on 3-D segmentation. In addition, this allows users to initiate multiple parallel segmentations without installing any software on their personal computer. Since we host the application in Azure, the application can also be directly connected to a hospital's picture archiving and communication system, allowing immediate segmentation of T1-weighted MRIs. The cloud is also directly connected to an AR-HMD, allowing direct visualization of the segmentation output in 3-D.

Clinical Applications

The currently described segmentation system could potentially be used to support AR navigation, particularly to guide a ventricular shunt placement.^{8,9} In this case, AR neuronavigation methods require accurate anatomical 3-D models to guide the intraventricular part of the trajectory. Furthermore, segmentation should also be reasonably fast to prevent disruption of clinical workflows. As the interest in AR neuronavigation has increased over the last years, segmentation techniques that are tailored to this modality are necessary. As our system operates completely automatically, is reasonably fast and accurate, can be connected to a hospital's picture archiving and communication system and can be accessed using AR-HMDs, we believe that it could fulfill this role. Furthermore, the system could benefit diagnostics and follow-up of cases of hydrocephalus.

Future Improvements

The currently described system has several potential improvements. First, to decrease the incidence of data-leaks, we will attempt to make the algorithm more sensitive to very thin boundaries between cavities. Very high-resolution scans of 400 by 400 pixels or more, which may be more common in the future, also would decrease the frequency of leaks. Furthermore, we aim to automatically recognize intraventricular blood, tumors, and the choroid plexus, which could also increase the accuracy of the

ventricles segmentation by using subtraction. Lastly, we have planned to add a postprocessing environment, in which the surgeon can manually improve the segmentation using boundary boxes, erasers and trajectory lines.

In the future, we will incorporate segmentation of T2-weighted images. This could potentially increase segmentation accuracy, as cerebrospinal fluid induces a high signal on this sequence. Previous studies using T2-weighted images have reported promising results.^{14,15} In addition, we want to explore the possibilities of segmenting CT scans to allow appliance in a wider range of clinical cases.

CONCLUSIONS

The currently described adaptive meshing-based segmentation algorithm provides accurate and time-efficient automatic segmentation of the ventricular system from T1 MRIs and direct visualization of the rendered surface models in AR. The

segmentation tool will benefit diagnostics and follow-up of hydrocephalus, regardless of the presence of a tumor. It can provide the basis for intraoperative AR-guided shunt placement system and AR neuronavigation for more extensive surgery, including the ventricular system.

CRediT AUTHORSHIP CONTRIBUTION STATEMENT

Jesse A.M. van Doormaal: Conceptualization, Methodology, Software, Formal analysis, Investigation, Visualization, Writing – original draft. **Tim Fick:** Conceptualization, Methodology, Formal analysis, Investigation, Writing – review & editing. **Meedie Ali:** Methodology, Investigation, Writing – review & editing. **Mare Köllen:** Investigation, Writing – review & editing. **Vince van der Kuip:** Investigation, Writing – review & editing. **Tristan P.C. van Doormaal:** Conceptualization, Methodology, Validation, Supervision, Funding acquisition, Writing – review & editing.

REFERENCES

- Alaraj A, Charbel FT, Birk D, et al. Role of cranial and spinal virtual and augmented reality simulation using immersive touch modules in neurosurgical training. *Neurosurgery*. 2013;72(suppl 1):115-123.
- Hooten KG, Lister JR, Lombard G, et al. Mixed reality ventriculostomy simulation: experience in neurosurgical residency. *Neurosurgery*. 2014;10:576-581.
- Panesar SS, Magnetta M, Mukherjee D, et al. Patient-specific 3-dimensionally printed models for neurosurgical planning and education. *Neurosurg Focus*. 2019;47:1-11.
- Ganguli A, Pagan-Diaz GJ, Grant L, et al. 3D printing for preoperative planning and surgical training: a review. *Biomed Microdevices*. 2018;20:65.
- Barsom EZ, Graafland M, Schijven MP. Systematic review on the effectiveness of augmented reality applications in medical training. *Surg Endosc*. 2016;30:4174-4183.
- Pelargos PE, Nagasawa DT, Lagman C, et al. Utilizing virtual and augmented reality for educational and clinical enhancements in neurosurgery. *J Clin Neurosci*. 2017;35:1-4.
- Triepels CPR, Smeets CFA, Notten KJB, et al. Does three-dimensional anatomy improve student understanding? *Clin Anat*. 2020;33:25-33.
- Li Y, Chen X, Wang N, et al. A wearable mixed-reality holographic computer for guiding external ventricular drain insertion at the bedside. *J Neurosurg*. 2019;131:1599-1606.
- Schneider M, Kunz C, Pal'a A, et al. Augmented reality-assisted ventriculostomy. *Neurosurg Focus*. 2021;50:1-7.
- González-Villà S, Oliver A, Valverde S, et al. A review on brain structures segmentation in magnetic resonance imaging. *Artif Intell Med*. 2016;73:45-69.
- Wu J, Zhang Y, Tang X. Simultaneous tissue classification and lateral ventricle segmentation via a 2D U-net driven by a 3D fully convolutional neural network. *Annu Int Conf IEEE Eng Med Biol Soc*. 2019;2019:5928-5931.
- Shao M, Han S, Carass A, et al. Brain ventricle parcellation using a deep neural network: application to patients with ventriculomegaly. *Neuroimage Clin*. 2019;23:101871.
- Zhang L, Wang X, Yang D, et al. Generalizing deep learning for medical image segmentation to unseen domains via deep stacked transformation. *IEEE Trans Med Imaging*. 2020;39:2531-2540.
- Ntiri EE, Holmes MF, Forooshani PM, et al. Improved segmentation of the intracranial and ventricular volumes in populations with cerebrovascular lesions and atrophy using 3D CNNs [e-pub ahead of print]. *Neuroinformatics*. <https://doi.org/10.1007/s12021-021-09510-1>, accessed February 19, 2021.
- Quon JL, Han M, Kim LH, et al. Artificial intelligence for automatic cerebral ventricle segmentation and volume calculation: a clinical tool for the evaluation of pediatric hydrocephalus [e-pub ahead of print]. *J Neurosurg Pediatr*. <https://doi.org/10.3171/2020.6.PEDS20251>, accessed February 19, 2021.
- Zhou X, Ye Q, Jiang Y, et al. Systematic and comprehensive automated ventricle segmentation on ventricle images of the elderly patients: a retrospective study. *Front Aging Neurosci*. 2020;12:618538.
- Jia H, Yap PT, Shen D. Iterative multi-atlas-based multi-image segmentation with tree-based registration. *Neuroimage*. 2012;59:422-430.
- Ellingsen LM, Roy S, Carass A, et al. Segmentation and labeling of the ventricular system in normal pressure hydrocephalus using patch-based tissue classification and multi-atlas labeling. *Proc SPIE Int Soc Opt Eng*. 2016;9784:97840G.
- Dubost F, de Bruijne M, Nardin M, et al. Multi-atlas image registration of clinical data with automated quality assessment using ventricle segmentation. *Med Image Anal*. 2020;63.
- Tang X, Luo Y, Chen Z, et al. A fully-automated subcortical and ventricular shape generation pipeline preserving smoothness and anatomical topology. *Front Neurosci*. 2018;12:321.
- Huo Y, Plassard AJ, Carass A, et al. Consistent cortical reconstruction and multi-atlas brain segmentation. *Neuroimage*. 2016;138:197-210.
- Kärkkäinen M, Wilkman T, Mesimäki K, Snäll J. Primary reconstruction of orbital fractures using patient-specific titanium milled implants: the Helsinki protocol. *Br J Oral Maxillofac Surg*. 2018;56:791-796.
- Snäll J, Narjus-Sterba M, Toivari M, et al. Does postoperative orbital volume predict postoperative globe malposition after blow-out fracture reconstruction? A 6-month clinical follow-up study. *Oral Maxillofac Surg*. 2019;23:27-34.
- Sigron GR, Rüedi N, Chamartin F, et al. Three-dimensional analysis of isolated orbital floor fractures pre- and post-reconstruction with standard titanium meshes and "hybrid" patient-specific implants. *J Clin Med*. 2020;9:1579.
- Chepurnyi Y, Chernohorskyi D, Zhukovtseva O, et al. Automatic evaluation of the orbital shape after application of conventional and patient-specific implants: correlation of initial trauma patterns and outcome. *J Oral Biol Craniofac Res*. 2020;10:733-737.
- Chepurnyi YV, Kopchak AV, Chernogorskiy DM, Zhukovtseva OI. Efficacy of application of a patient-specific implants in treatment of the orbit walls defects, combined with a cheekbone complex fractures. *Klin Khir*. 2020;87:65-70.

27. Saloniemi M, Lehtinen V, Snäll J. Computer-aided fracture size measurement in orbital fractures—an alternative to manual evaluation [e-pub ahead of print]. *Craniomaxillofac Trauma Reconstr*. <https://doi.org/10.1177/1943387520962691>, accessed March 2, 2021.
28. Dice LR Measures of the amount of ecologic association between species. *Ecology*. 1945;26: 297-302.
29. Huttenlocher DP, Klanderman GA, Rucklidge WJ. Comparing images using the hausdorff distance. *IEEE Trans Pattern Anal Mach Intell*. 1993;15:850-863.
30. Shao M, Han S, Carass A, et al. Shortcomings of ventricle segmentation using deep convolutional

networks. *Underst Interpret Mach Learn Med Image Comput Appl* (2018). 2018;11038:79-86.

31. Iglesias JE, Sabuncu MR. Multi-atlas segmentation of biomedical images: a survey. *Med Image Anal*. 2015;24:205-219.
32. FsTutorial - Free Surfer Wiki. Available at: <https://surfer.nmr.mgh.harvard.edu/fswiki/ReconAllRunTimes>. Accessed March 24, 2021.

Conflict of interest statement: This project has received funding from the Eurostars-2 joint programme with co-

funding from the European Union Horizon 2020 research and innovation programme (114221 Sapiens3D). T.P.C. van Doormaal is founder and CMO of Augmedit, a start-up company that develops Augmented Reality tools for surgeons.

Received 20 May 2021; accepted 21 July 2021

Citation: *World Neurosurg*. (2021) 156:e9-e24. <https://doi.org/10.1016/j.wneu.2021.07.099>

Journal homepage: www.journals.elsevier.com/world-neurosurgery

Available online: www.sciencedirect.com

1878-8750/© 2021 The Authors. Published by Elsevier Inc. This is an open access article under the CC BY license (<http://creativecommons.org/licenses/by/4.0/>).

APPENDIX

GUIDELINES FOR MANUAL SEGMENTATION

Accuracy of expanding-mesh ventricles segmentation - Protocol for manual segmentation of the ventricular system

Introduction

The ventricular system is an anatomically complex 3-dimensional structure that has a distinctive shape on a magnetic resonance imaging (MRI) scan. As the structure is filled with cerebrospinal fluid, the system is either completely black (T₁) or white (T₂) on an MRI scan, and forms a continuous cavity. The ventricular system consists of 4 segments, whereas the lateral (first and second) ventricles connect to the third ventricle using the foramen of Monro. The third ventricle connects to the fourth ventricle using the aqueduct of Sylvius.

Although the structure can be recognized by the human eye on MRI scans, no commercially available systems for the fully automatic segmentation of the structure have been developed. This project aims to develop a fully automatic back-end function for medical segmentation software that can segment, among other brain structures, the complete ventricular system. To scrutinize the accuracy of this algorithm, an extensive benchmark set of optimally segmented ventricular system 3-dimensional (3-D) data is needed. This can then be used to compare volumes and surface geometries of automatic segmentation to, functioning as a “golden standard.” As 3-D segmentation of MRI scans is a relatively new field of study, this dataset is currently not available. For this reason, we will manually segment the ventricular system from 46 MRI scans as a kick-off for this study, to create our own extensive benchmark set.

Although manual segmentation is relatively straightforward, it is very important to carry out correctly for a proper analysis. Furthermore, it is imperative to establish a set of rules to keep the segmentation method homogenous between researchers. This document will function as a guideline for the standard method of manual segmentation.

Instruction

Software/Hardware Requirements.

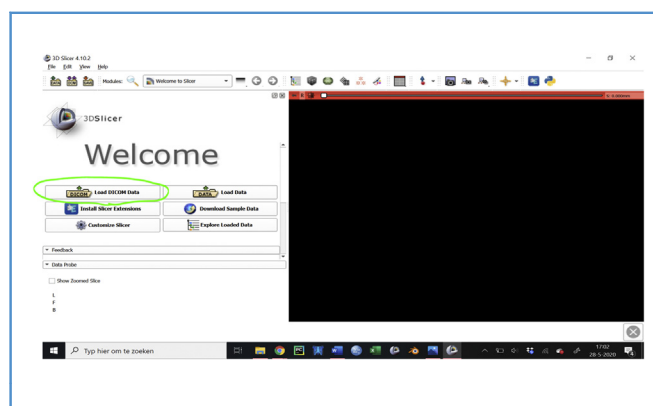
The following materials are needed:

- A hospital PC within secured network, including mouse, preferably with a graphical processing unit;
- 3D slicer version 4.10.2 (install software before further steps using the link: <https://www.slicer.org/>);

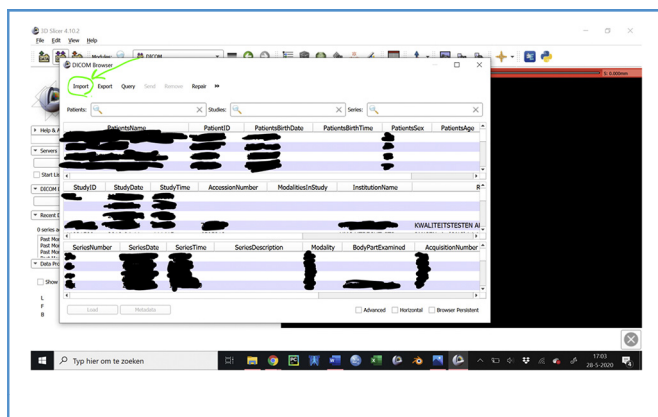
- Digital Imaging and Communications in Medicine data of the MRI set to be segmented; and
- Optional: graphical tablet/touchscreen stylus (if the laptop being used has a touchscreen)

Instructions

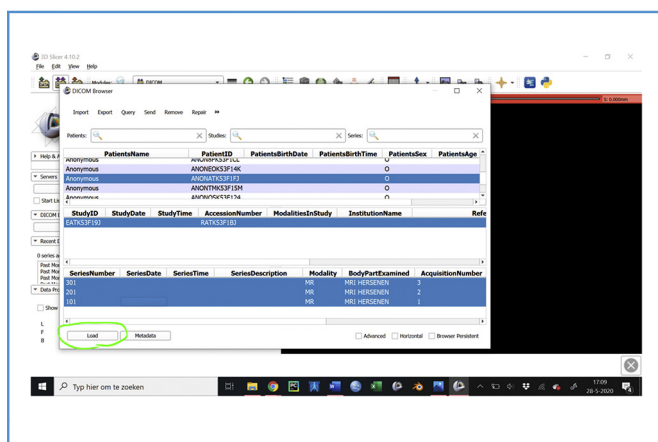
1. First, de-encrypt the anonymized data. Open the USB stick, doubleclick the “USB Security” icon and insert the password provided by us.
2. After de-encryption, load up 3-D slicer. Press the “Load DICOM Data” button.



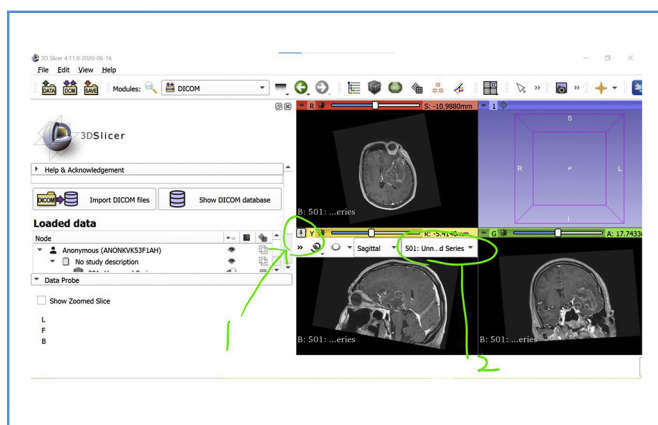
3. Press the ‘import’ button. Select the directory of the transversal T₁ + contrast series of your patient, as described within the ‘metadata’ sheet (In.xlsx format), and press ‘Import’ again. Verify that the number of your chosen patient (which you can find under the folder name) corresponds to the number under ‘PatientNumber’ in the metadata sheet.



4. Select the transversal T1 + contrast sequence in the bottom table. Verify that you've selected the right sequence by verifying the 'SeriesNumber,' 'Modality,' and the 'SeriesDescription' with your metadata sheet. Then, press the 'Load' button.



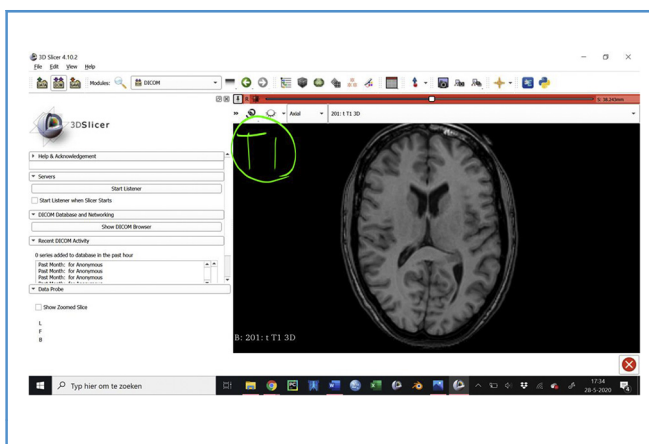
5. First, check the imported sequence for the patient in the viewing window. This can be done by selecting the right sequence using the pin icon and the dropdown menu on the right.



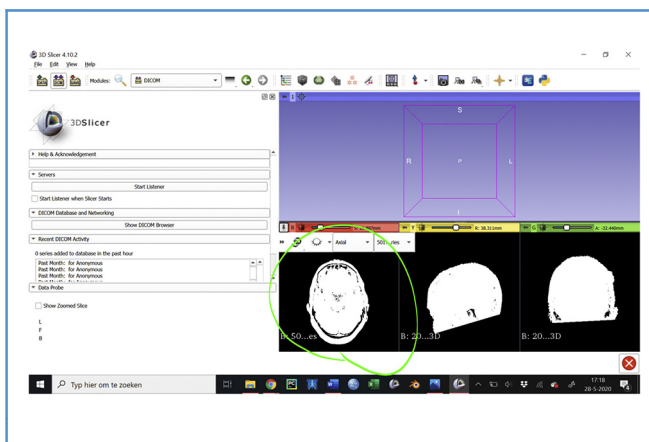
Verify that a good resolution transversal T1 + contrast sequence is available that includes the complete ventricular system.

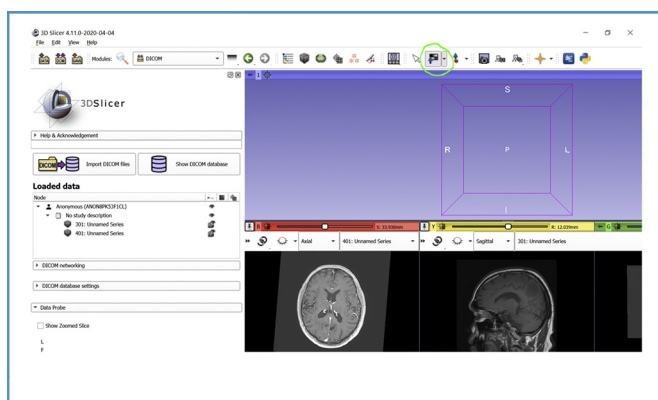
The ventricular system should be distinctly visible. However, it is no reason for exclusion if the system is partly compressed by a tumor. The series should include at least 64 slices, more is better.

Example of a good scan:

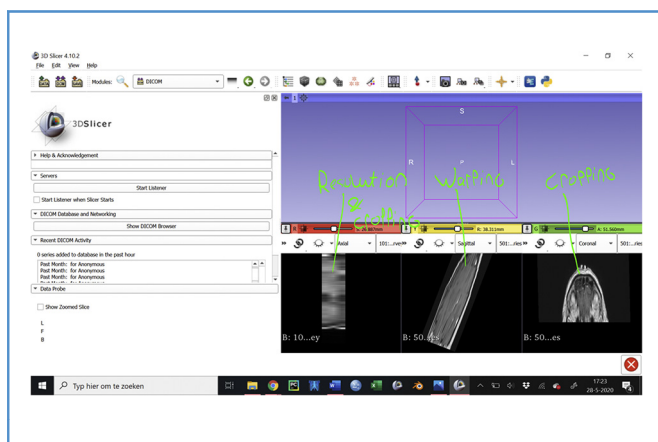


During importing, several problems can occur. The most common problem is bad windowing: The scan appears completely white. This can often be fixed by changing the windowing level by enabling the 'windowing' button and clicking and dragging the mouse over the scan viewer window. Dragging the mouse horizontally changes the window width, while dragging the mouse vertically changes the window level. For more information on windowing, check <https://radiopaedia.org/articles/windowing-ct>.

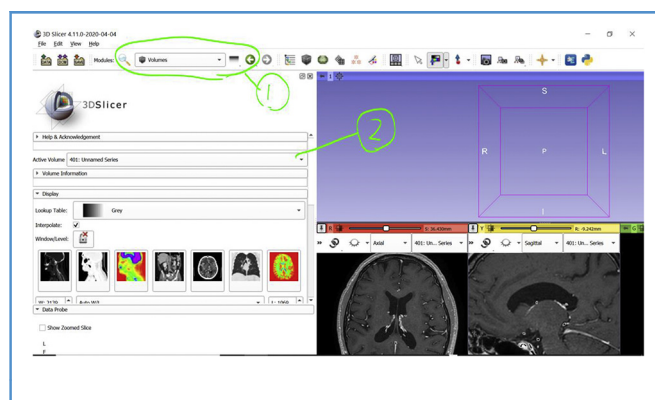




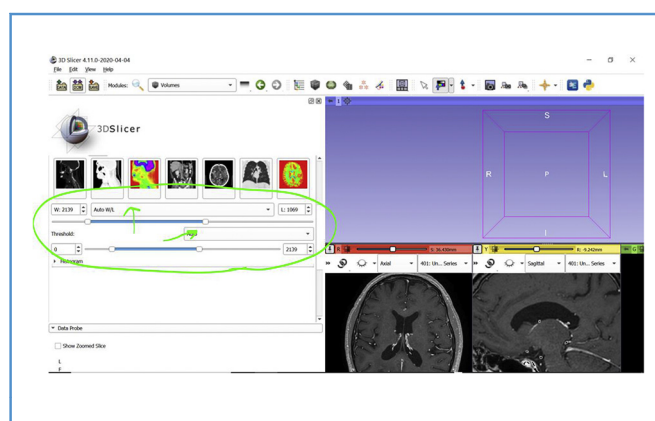
Other problems that can occur are bad resolution, warping (the image looks stretched/compressed over one or more axes), and volume cropping (the image is only partially visible). First, check if any other good-quality T1 series are available within the patient data folder (preferably with contrast, but no contrast is also acceptable if no good contrast series are available). If these problems occur for all series, try reimporting. If the issue cannot be fixed for all series, omit the patient and report the case as omitted by writing a 'Y' in the cell under the column 'Excluded' in your metadata sheet.



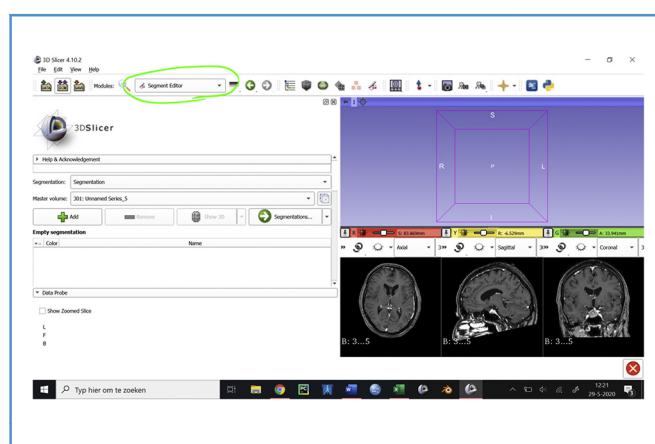
6. Next, we'll standardize the windowing settings. For this, select the 'volumes' module under the dropdown menu in the toolbar. Check whether the series number under 'Active Volume' matches your series. If not, change it using the dropdown menu.



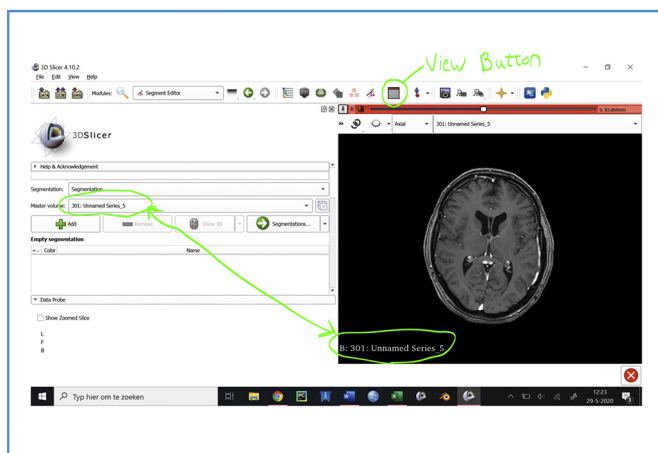
Now, choose the 'auto' setting for both level and width. For this, scroll down use the dropdown menus above the bottom 2 sliders of the module. You can lock the windowing settings using the 'lock' button.



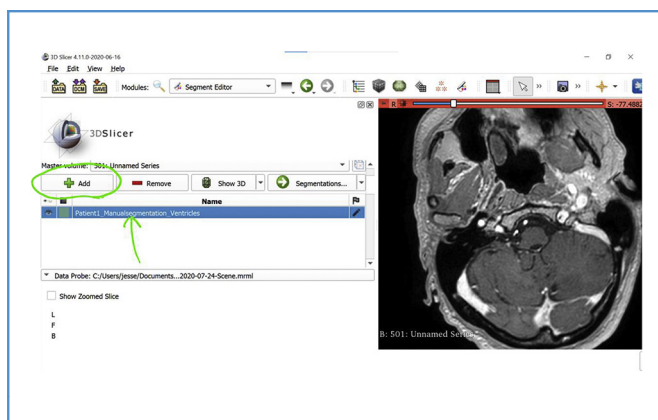
7. Now, you can start manual segmentation. First, you'll have to create a new segmentation. For this, select 'segment editor' in the dropdown menu at the top of your screen.



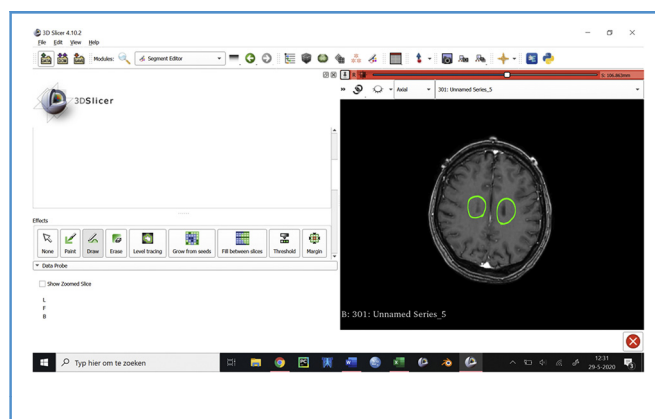
8. After you have opened the segmentation menu, first verify that you have selected the right series. For this, the name under 'master volume' and your selected series should match. For a better view, select 'red slice only' under the view button in the toolbar.



9. If all is correct, create a new segmentation using the 'add' button. Name the segmentation by double clicking using the following name format:
Patient*Number*_Manualsegmentation_Ventricles.



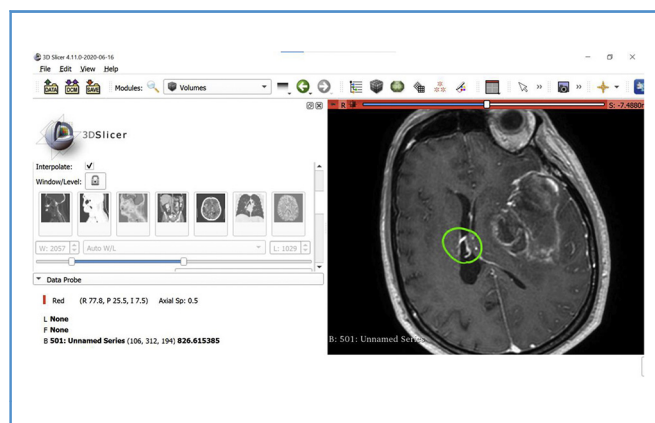
10. Next, scroll down until you see the 'effects' menu. Here, select the 'draw' function. Start at the most superior slice where you can start seeing the lateral ventricles. Change slices by scrolling. When you have decided to start segmenting, start the stopwatch. If you need to take a break during segmentation, pause the stopwatch during the break.



11. You can now trace the outline of the ventricle using your mouse or a stylus. Be sure to work slowly and carefully; accuracy is key. It will help to zoom the image using the ctrl key and the mouse wheel. You can drag the image by pressing the middle mouse button. You can hide the segmentation menu using the small 'x' in the module top right corner.

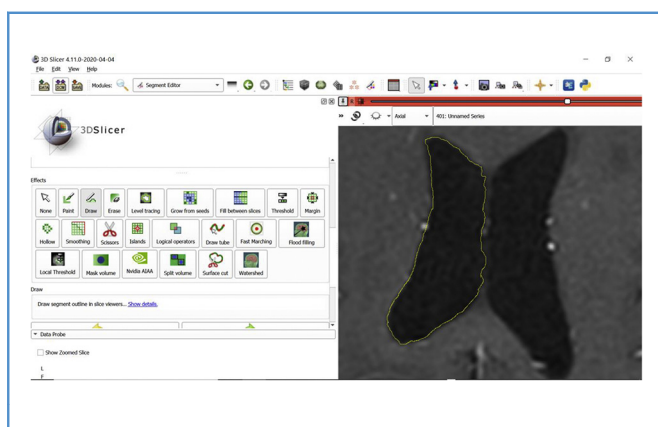
There are certain rules to follow during segmentation, as stated in the following list:

- The choroid plexus is not part of the segmentation and should be avoided if possible.

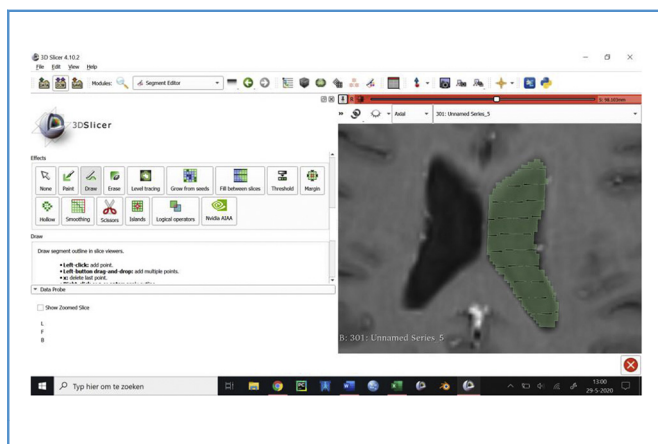


- There is often no sharp border between the intraventricular space and the brain matter, which is caused by the ependyma. Always strive to include only the black cerebrospinal fluid in your segmentation.
- Always use the 'auto windowing' settings during segmentation, and do not change windowing settings between slices. This provides a standardized view of the ventricular space.

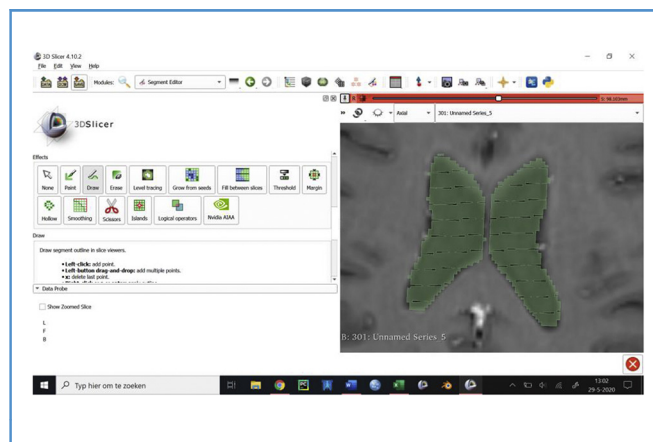
- Always use the axial view for initial segmentation.
- Stop segmenting inferior of the choroid plexus of the fourth ventricle. If you're in doubt where exactly to stop, it is better to keep segmenting a little bit inferior of the fourth ventricle, as we can trim this later.



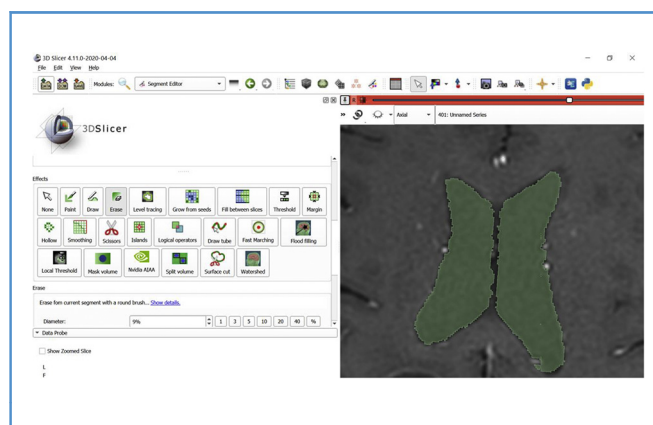
12. Later, you can still manually edit the surface, so it does not have to be perfect. After tracing the complete outline, click the right mouse button within the outline to add a surface.



You can now repeat steps 9 and 10 for separate outlines, for example for the contralateral ventricle.

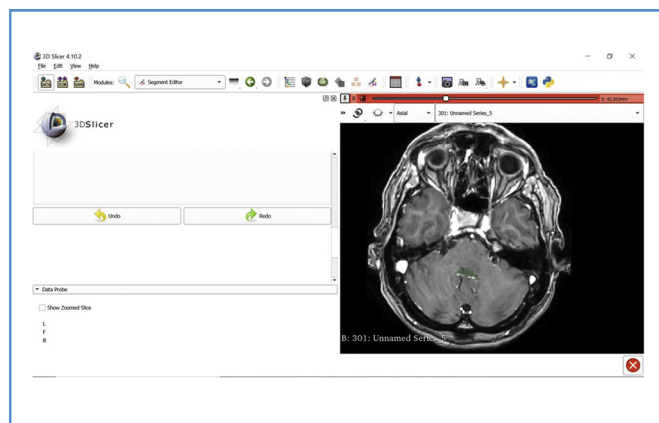


13. As you may have noticed, the segmentation is far from perfect. You can now improve the surface using the 'paint' function. This creates a brush you can use to paint missing parts. You can increase/decrease the brush radius using shift + scrolling. Try experimenting with the different sizes; large brush sizes are better for filling the holes, smaller brush sizes are better for details. You can also use the 'erase' function to erase parts. Do not use the other functions.

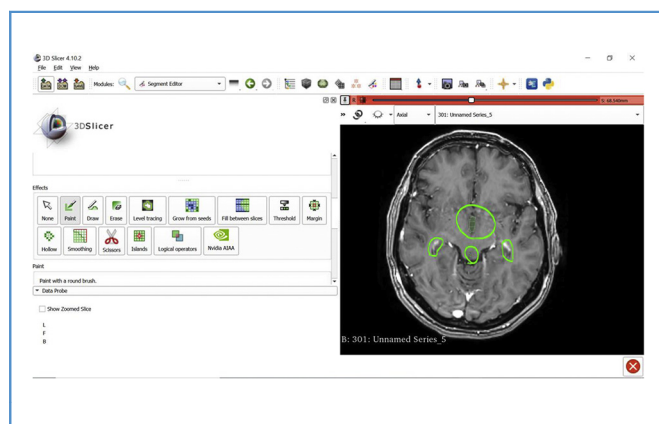


You will notice a 'stair' effect being present on your surface. To a certain degree, this is unavoidable and will be smoothed out during exporting.

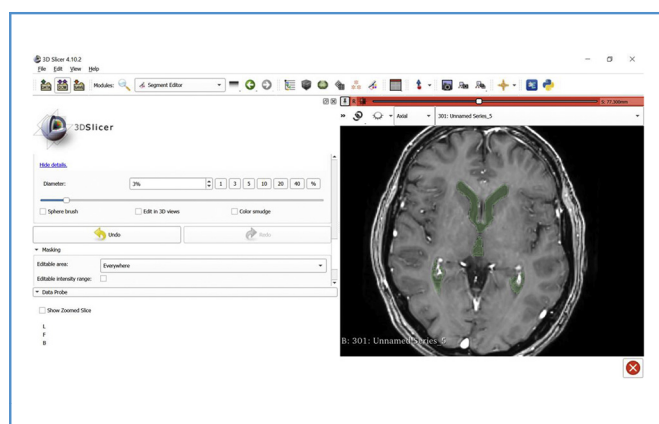
14. Repeat the segmentation for every slice where the ventricles are visible. The following pictures give an overview of the ventricular system segments that you should segment in different levels of the brain (note the green segmentation):



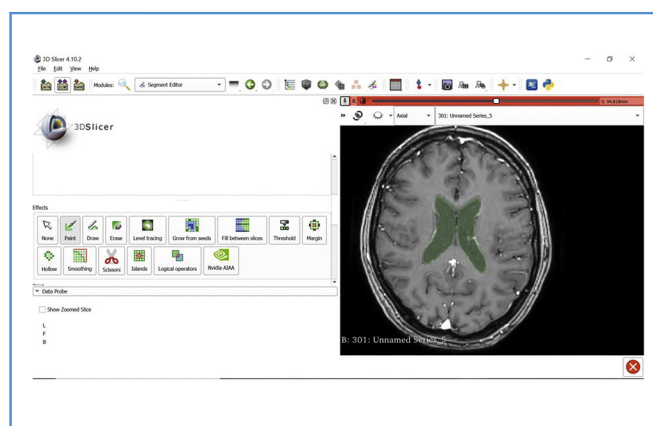
Inferior part of fourth ventricle



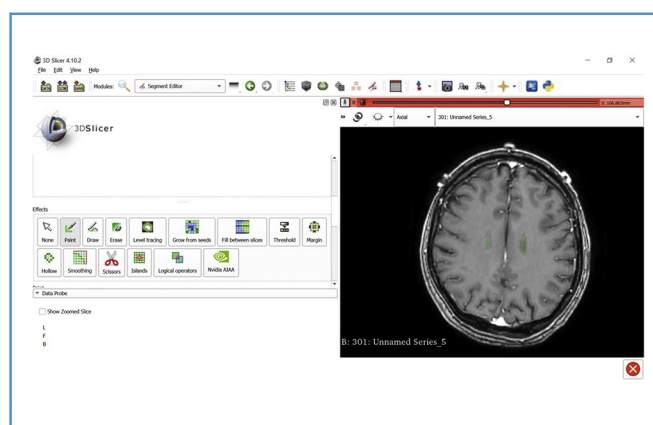
Aqueduct, inferior part of third ventricle, and temporal horns (often too small to segment)



Lateral ventricles, third ventricle, and temporal horns

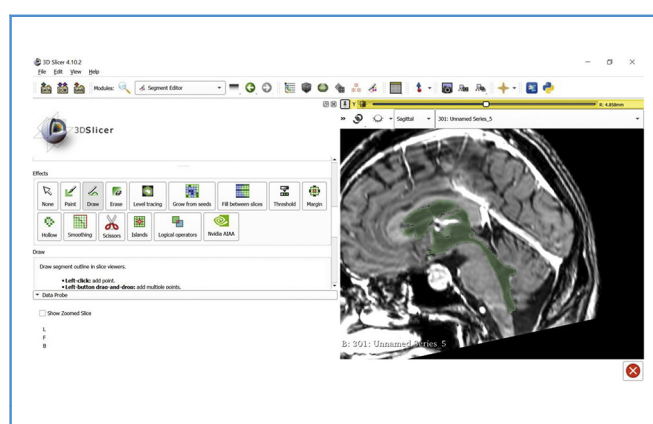


Lateral ventricles

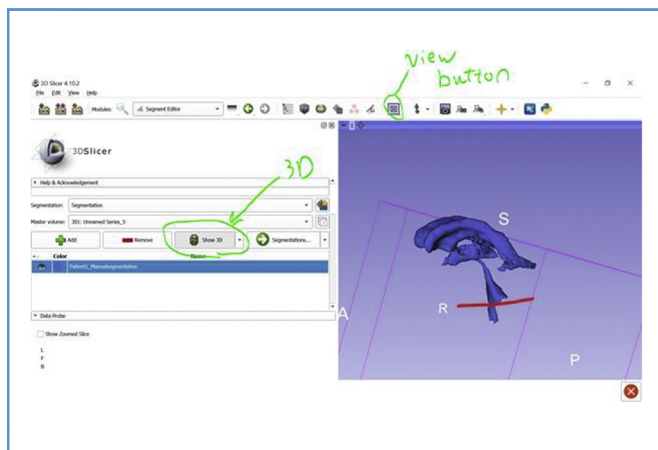


Superior part of lateral ventricles

15. After completing the process for all slices, check and correct the shape for the coronal and sagittal direction using the brush. Do not skip this step, as corrections in the different directions often significantly improve the shape of the model.



16. Check the segment isosurface in 3D by pressing the 'show 3D' button under the segmentation menu. Make sure to enable the 3D viewer using the viewer button in the toolbar. If necessary, you can trim your ventricle at the level of the inferior border of the choroid plexus of the fourth ventricle.

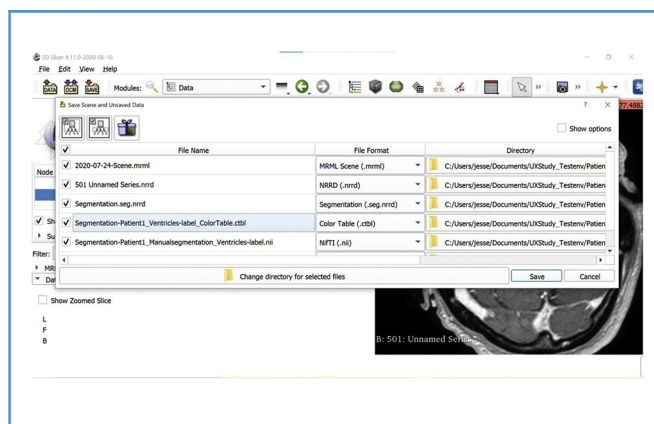


17. If you are satisfied with the result, it is time to save your segmentation. First, stop the stopwatch and note the time in seconds in the metadata sheet under 'TTC' (Time-to-completion). Then, we convert the segmentation to a binary labelmap. For this, open the 'Data' module under the dropdown menu in the toolbar. Then, scroll to your segmentation data under 'Node.' Then, right click and select 'Export visible segments to binary labelmap.' This will create a new data array.

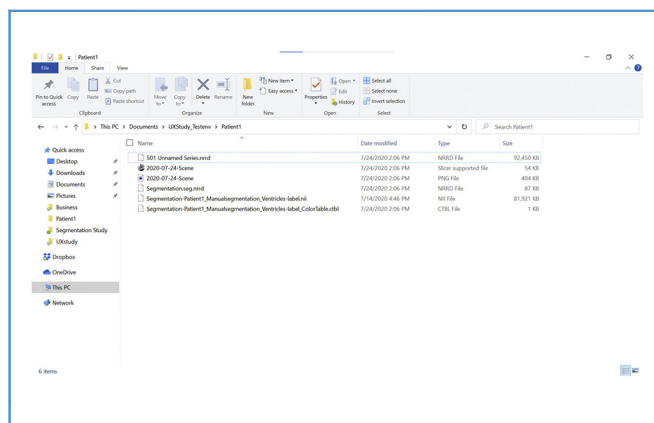


18. Then, all files should be saved within the appropriate patient folder on the USB. Do not bury the files in additional folders (e.g., within the T1 + contrast folder), as our statistics script only automatically detects folders within the top-level patient folders. Save all 3dslicer data to the folder using the 'file'

button in the top left corner. This will open the 'Save Scene and Unsaved Data' module. This contains the scene (in.mrml format standard), the scan series (in.nrrd format standard), your segmentation (in.seg.nrrd format standard), the binary labelmap (in.nrrd format standard) and the label ColorTable (in.ctbl format). You need to change the format of your binary labelmap to.nii data using the dropdown menu. The save menu should look like the following screenshot:



In the patient folder on the USB, remove all original scans; in other words, only the data you created should remain within the patient folder. The saved datafolder should look similar to the following screenshot:



It is important to verify this, as the statistics script will automatically recognize this data structure. As a final step, add the full name of the binary labelmap to the metadata file under the column 'ManualSegmentationDir.' The column 'AutomaticSegmentationDir' can be left empty.

19. All done! Encrypt all new data. We will provide physical pick-up of the data.